Locking Zipper-Coupled Origami Tubes for Deployable Energy Absorption

Zhongyuan Wo
Deployable and Reconfigurable Structures Laboratory,
Department of Civil and Environmental Engineering,
University of Michigan,
Ann Arbor, MI 48109
e-mail: wozhy@umich.edu

Julia M. Raneses
Deployable and Reconfigurable Structures Laboratory,
Department of Civil and Environmental Engineering,
University of Michigan,
Ann Arbor, MI 48109
e-mail: jraneses@umich.edu

Evgueni T. Filipov[1]
Deployable and Reconfigurable Structures Laboratory,
Department of Civil and Environmental Engineering;
Department of Mechanical Engineering,
University of Michigan,
Ann Arbor, MI 48109
e-mail: filipov@umich.edu

Energy absorption devices are widely used to mitigate damage from collisions and impact loads. Due to the inherent uncertainty of possible impact characteristics, passive energy absorbers with fixed mechanical properties are not capable of serving in versatile application scenarios. Here, we explore a deployable design concept where origami tubes can extend, lock, and are intended to absorb energy through crushing (buckling and plasticity). This system concept is unique because origami deployment can increase the crushing distance between two impacting bodies and can tune the energy absorption characteristics. We show that the stiffness, peak crushing force, and total energy absorption of the origami tubes all increase with the deployed state. We present numerical and experimental studies that investigate these tunable behaviors under both static and dynamic scenarios. The energy-absorbing performance of the deployed origami tubes is slightly better than conventional prismatic tubes in terms of total absorbed energy and peak force. When the origami tubes are only partially deployed, they exhibit a nearly elastic collapse behavior; however, when they are locked in a more deployed configuration, they can experience non-recoverable crushing with higher energy absorption. Parametric studies reveal that the geometric design of the tube can control the nonlinear relationship between energy absorption and deployment. A physical model shows the potential of the self-locking after deployment. This concept for deployable energy-absorbing origami tubes can enable future protective systems with on-demand properties for different impact scenarios.
[DOI: 10.1115/1.4054363]

Keywords: energy absorption, deployable structures, origami, origami crushing and buckling

Introduction

Conventional energy absorption systems serve as passive sacrificial structures that absorb the kinetic energy of an impact through buckling, crumpling, and plastic deformation. Thin-walled prismatic tubes and cellular structures are effective in this role because they can provide a large amount of energy absorption for their small overall mass [1]. The energy absorption characteristics of such structures are typically evaluated from quasi-static compressive tests where the crushing distance (δ), mean crushing force (P_m), and peak crushing force ($P_{\max}$) are of primary interest (Fig. 1(*a*)). The total energy that can be absorbed by the system is $\delta \cdot P_m$, while the peak crushing force is of interest as it correlates with the forces and accelerations translated to the object that is to be protected.

One recent innovation for energy-absorbing tubes has been to use origami inspired patterns in the design and fabrication of the thin-walled structures [2]. The pre-patterned geometry triggers controlled buckling modes during crushing, which in turn can reduce the peak forces and increase the total amount of energy absorbed (Fig. 1(*b*)). Origami can also offer a variety of geometric design options and can have the benefit of easy fabrication from a flat developable surface [3–5]. For example, a thin-walled tube with pre-folded Yoshimura pattern [6] and a sandwich-like structure with Kresling pattern [7] can both provide favorable energy-absorbing behaviors. However, all of these previous origami systems are passive, and the entire energy absorption performance is determined by the design geometry and material properties.

In this paper, we present a concept that takes further advantage of the origami principles and uses the folding kinematics of zipper-coupled tubes [8] to enable deployment and tuning of the energy absorber. By deploying the origami, it becomes possible to initiate earlier contact between colliding objects and to increase the crushing distance (δ) of the system. The longer crushing distance allows for an increase in the amount of absorbed energy if we assume that forces would be in the same range (Fig. 1(*c*)). Additionally, a deployable energy absorber could be stowed compactly prior to impact in order to save onboard space or improve the aerodynamics in vehicle applications.

Deployment of the origami tubes also enables tunable performance of the energy absorber as shown conceptually in Fig. 1(*d*). The proposed structures have the potential to deploy, lock, and crush at different geometric states where each state offers drastically different force–displacement characteristics. Our results, presented later in the paper, show that the crushing distance (δ), mean crushing force (P_m), and peak crushing force ($P_{\max}$) can all be increased by elongating the origami tubes. Depending on the mass and velocity of an impacting object, the energy absorber could be deployed to minimize the peak force and absorb only the desired amount of kinetic energy (Fig. 1(*d*)).

The deployable origami structures explored in this paper share similarities with other energy absorber designs in the emerging field of mechanical metamaterials [9–11]. Similar to the proposed origami structures, the programable behavior of these metamaterials is a function of their design and geometric architecture. However, the proposed systems are also fundamentally different. In contrast to designs that store and dissipate energy through elastic behaviors [11], the proposed origami tubes are non-recoverable and energy is

[1]Corresponding author.
Contributed by the Mechanisms and Robotics Committee of ASME for publication in the Journal of Mechanisms and Robotics. Manuscript received October 20, 2021; final manuscript received April 14, 2022; published online May 2, 2022. Assoc. Editor: Chin-Hsing Kuo.

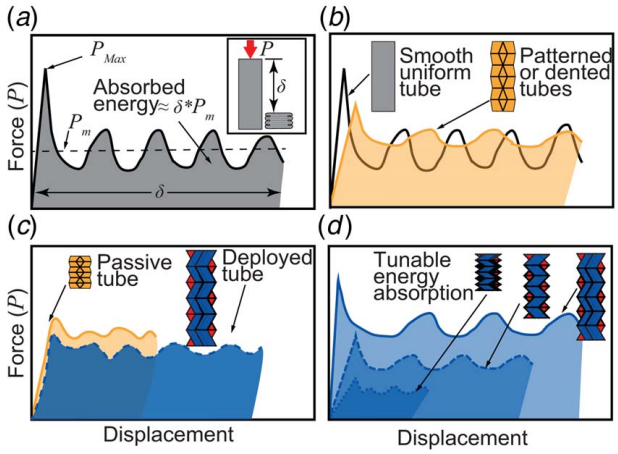

Fig. 1 Conceptual force–displacement curves of different energy-absorbing tubes. (*a*) A prismatic tube has a high peak force for crushing (P_{max}) with the total absorbed energy represented by the area underneath the curve ($\approx\delta \cdot P_m$). (*b*) Introducing origami patterns in the design can reduce the peak force while increasing the total energy absorbed [2]. (c) The proposed origami tubes here could deploy to increase the crushing distance δ while remaining stowed prior to use. The increased crushing distance could allow for more energy absorption than a passive system with comparable peak forces. (*d*) Deployment of the proposed tubes can tune the initial stiffness, the peak forces, and the total absorbed energy.

absorbed through crushing, buckling, and plasticity in the thin sheets (non-recoverable, but a lighter and more efficient method for energy absorption). The potential capability for deployment is also different because the origami tubes could increase the crushing distance and enable on-demand tuning of the system behavior.

This work serves as an initial demonstration and a proof-of-concept for the deployable origami tube energy absorbers. To present their capabilities, this paper is structured as follows: first, the geometry, material properties, and fabrication of the origami tubes are discussed with an emphasis on locking the tubes into a specific state. Next, a finite element (FE) model is introduced to study the energy absorption behavior. The experimental setup for quasi-static and dynamic drop tests are then described. A series of quasi-static experiments are performed to quantify the energy absorption behavior of the tubes at different states of deployment. The effect of tube locking on the energy performance is explored by simulating tube crushing with only one or both ends of the tube restrained. Analytical simulations of the systems allow for a comprehensive parametric study, which explores the performance and tunable designs offered by various geometries of the tube. A series of dynamic drop tests are used to demonstrate the tunable stiffness and its influence on the initial impact. Next, a prototype of the zip-tie mechanism is integrated into a physical model to enable self-locking. Finally, the concluding remarks summarize the results, present limitations of the current study, and emphasize topics for further research including the deployment mechanisms and the physical fabrication of the proposed energy absorbers. An earlier version of this study was presented by the authors in a conference publication [12], while the work presented here contains a more extensive numerical and experimental exploration of the energy-absorbing tubes.

System and Methods

Geometry, Fabrication, and Locking of Origami Tubes. The geometry of the proposed deployable energy-absorbing tubes originates from the popular "Miura-ori" origami pattern. This pattern was first explored as a way to package large membranes and deploy them in outer space [13]. The Miura-ori has been applied in various engineering disciplines, such as the self-locking metamaterials [14] and the deployable canopies [15]. The Miura-ori pattern is developable making it easy to fold directly from a flat sheet. It is flat foldable so it can be stowed compactly and is rigid foldable which allows for fabrication with rigid panel components connected by flexible hinges. The structure also has one-degree-of-freedom (DOF) origami kinematics which allows for a prescriptive longitudinal deployment where only the hinges (or folds) deform. Finally, the zipper-coupling concept for Miura-ori tubes adds stiffness to the origami structure [8], which makes it possible to lock the system and crush it as will be discussed further.

The geometric definition of the Miura-ori pattern and zipper tubes begins by prescribing the dimensions of the unit cell (Fig. 2(*a*)). The unit cell is formed by four identical panels connected at a vertex, with each panel defined by a height a, width c, and vertex angle α (the acute angle of the parallelogram). This unit cell can be folded into a three-dimensional shape where the current geometric configuration is governed by the dihedral folding angle $\theta \in [0, \pi]$.

The zipper-coupled tube system (Fig. 2(*b*)) is constructed by repeating and connecting symmetric Miura-ori cells. Instead of the dihedral angle, it is more intuitive to use a percentage of extension to define the longitudinal configuration of the tubes. The percentage equals to the ratio of current length to the maximum extended length, which is the product of the number of segments (N) and the panel width (c). The tube is thus fully deployed when the extension is 100% ($\theta = \pi$) and packed into a compact size when the extension is 0% ($\theta = 0$). This structure has only one flexible deformation mode through which it can be deployed with bending around the fold lines. Other deformation modes require engagement of panel bending and stretching, which significantly increases the stiffness of the system [8].

The zipper tubes were manually folded and glued from laser-cut polyester Mylar® sheets with a thickness of 0.127 mm. Based on a prior work [16], the tubes for all experimental tests consist of six segments, with their planar geometry set to be $a = c = 25$ mm and $\alpha = 55$ deg. The systems were locked by constraining both ends with significantly thicker 5 mm acrylic plates.

Fabrication of the locked zipper tubes consists of four major steps (Fig. 2(*c*)). First, two Miura-ori patterns with three units (six segments) are perforated by a Universal Laser System (VLS 6) and folded into a 3D shape. These two Miura-ori sheets are then flattened again and glued in the zipper orientation (step 1). This assembly is folded into a 3D shape and two additional Miura-ori sheets are glued to form the complete unlocked zipper tubes (step 2). Specifically, one sheet is rotated and glued to the other in a zig-zag manner, and a prior work [8] illustrated the connection in its second figure. This system can fold and unfold freely to different states (step 3). The zipper tubes are designed with tabs on both ends that are glued to two square acrylic plates to lock the tubes (step 4). The connections between zipper tubes and acrylic plates were made by gluing the two parts together with a LOCTITE® bonding system. The tabs are continuous with the base sheet and are perforated to fold orthogonally against the acrylic plate. Therefore, the relative translation between the zipper tubes and the acrylic plate is restrained, while the edges of the tube are free to rotate relative to the plate. When this connection with the endplates is complete, the structure is locked and can no longer fold without crushing.

We explored zipper tube systems locked at three different levels of extension, ~50%, ~75%, and ~95%. These extensions are chosen to represent a half, three quarters, and near fully deployed systems. A 100% deployed structure is not feasible because it is completely flat ($\theta = \pi$). Seven tubes were fabricated for each of the three desired extension ranges. Due to manufacturing error, the tubes aimed at half extension (~50%) averaged at 52%, those at the three-quarters extension averaged at 72%, and those at the high extension averaged at 95%. In the subsequent text, we use these averaged extensions to represent the systems folded at the three different extensions.

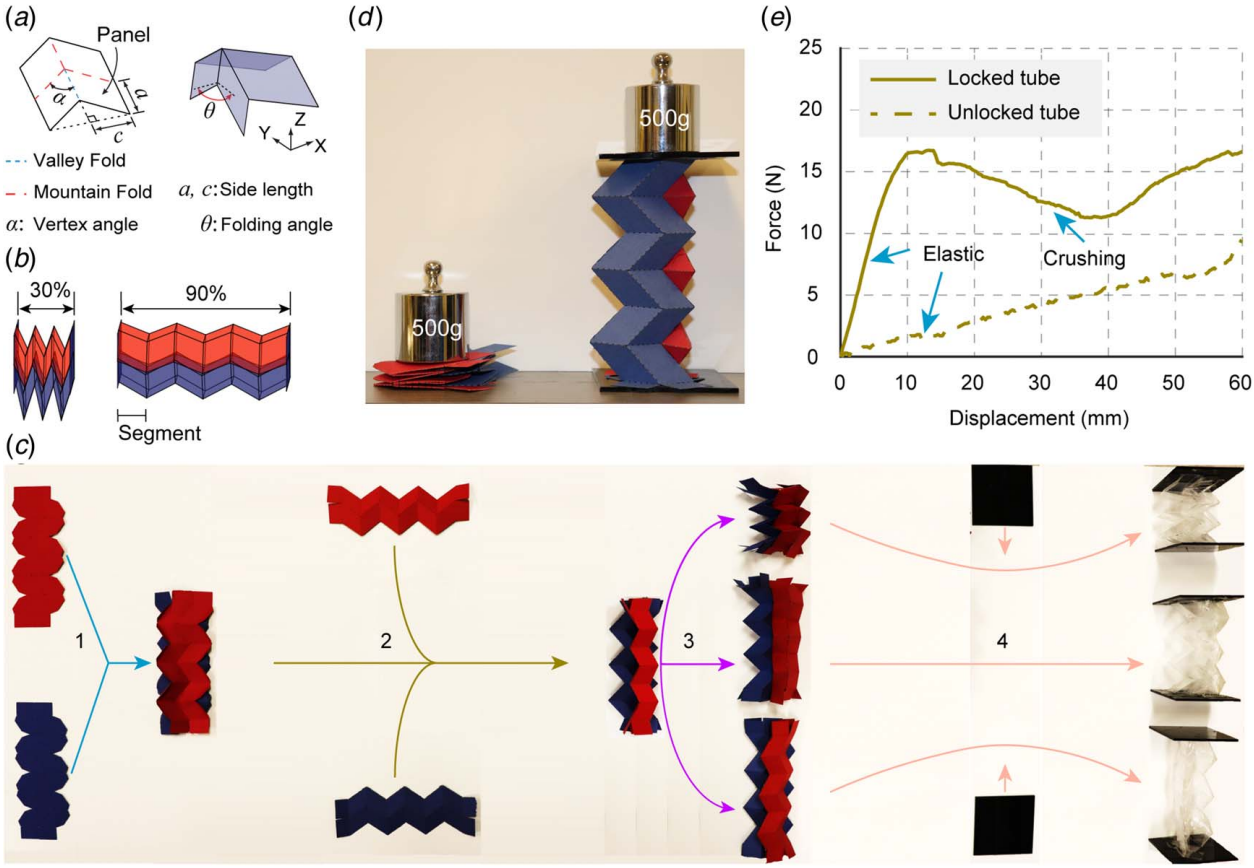

Fig. 2 Geometry, fabrication, and locking. (*a*) A unit cell of the Miura-ori pattern is defined by side lengths *a*, *c*, vertex angle α, and folding angle θ. (*b*) Zipper tubes at 30% and 90% extension with one segment indicated. (*c*) Fabrication process of locked zipper tubes. Paper tubes are shown on the left for visual clarity, and a final tube made from polyester sheets is shown on the right. (*d*) Comparison of load bearing capacity between unlocked (left) and locked (right) zipper tubes. Locking restricts the kinematic motion and makes the structure significantly stiffer. (*e*) Axial loading response in quasi-static experiments for locked and unlocked tubes. The locked structure ultimately crushes resulting in the nonlinear response.

To demonstrate the importance of locking on the axial stiffness, in Fig. 2(*d*), we present two identical zipper tubes made with construction paper. The locked structure weights 8.6 g and can support a mass of 500 g without a visible deformation (58 times its own weight), while the unlocked structure collapses into a flat state by following the one DOF folding kinematics. We also make a quantitative comparison of the axial loading response between locked and unlocked tubes (Fig. 2(*e*)), where the tests are conducted on polyester prototypes. For the locked tube system, the ends are constrained with acrylic plates. The initial stiffness of the two cases is drastically different. The locked tube has an initial stiffness of 1.8 N/mm, while the unrestrained tube has a stiffness of 0.2 N/mm. The unrestrained tube does not have a zero stiffness and has a generally elastic response because the folds of the system remain elastic, and fabrication imperfections (e.g., adhesive at fold vertices) restrict the perfect kinematic motion of the Miura-ori pattern. These preliminary tests show the large difference that can be obtained by locking the ends of the tubes. We then explore the nonlinear axial crushing of these systems in the subsequent sections.

Finite Element Model. In this paper, we use a finite element model (ABAQUS/Explicit [17]) that consists of shells elements and rotational hinges as the basis for numerical simulation. The origami panels are meshed with *S*4 general purpose shell elements (Fig. 3(*a*)). Adjacent panels are connected via connector elements (hinges) with prescribed rotational stiffness to simulate the bending behavior of fold lines. Each end of the thin tube system is connected to a plate with significantly higher stiffness to restrain translational movements.

In the simulation, the crushing of locked zipper tubes is modeled as axial compression between two rigid plates. One of the rigid plates is set to be completely fixed by restraining all six DOFs, while the moving plate is constrained to only translate along the axial direction of the zipper tubes. The crushing process is controlled by assigning a prescribed downward displacement to the moving plate, in which the moving rate is applied using a smooth amplitude definition. Self-contact (surface to surface) is applied to model contact between different parts of the zipper tubes and rigid plates. Friction resulting from contact is considered in the model with a coefficient of friction of $\mu = 0.25$. The reaction force in the axial direction is monitored in each simulation step and is recorded with respect to the position of the top plate. The force–displacement data are then used to calculate absorbed energy, mean force, and maximum force. Convergence with respect to the mesh size is examined, and a mesh size of 2.5×2.5 mm is chosen because it is able to provide a strain energy solution that is within 2% of a mesh with 1×1 mm elements. The simulation time is set to be 20 ms to keep the ratio of kinetic energy to strain energy under 5% so the dynamic effects can be considered as negligible to the global response.

Material properties for the polyester films are assumed to be isotropic. Young's modulus is set to be $E = 4.4$ GPa based on the material tests, and Poisson's ratio is assumed to be $\nu = 0.33$. The model dimensions and thickness are set to be the same as the physical models that were fabricated. The rotational stiffness (K_l) of the folds can vary dramatically due to the variation in materials, fabrication, and folding history. Previous research [18,19] reveals that (K_l) is expected to be proportional to the length of fold lines and

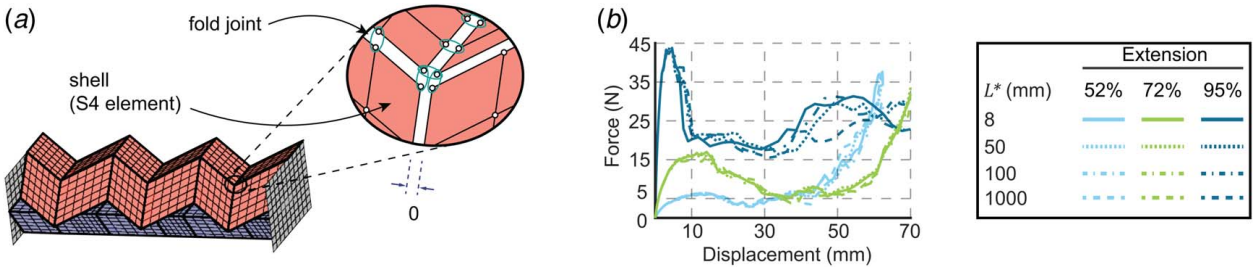

Fig. 3 Finite element model. (*a*) The zoom-in figure on top shows the details of the connections between adjacent panels. Finite element model of the locked zipper tubes on the bottom is only representative and a finer mesh is used for the analyses. (*b*) Axial force–displacement simulation for the locked zipper tube with different length scale parameters *L.**

the bending stiffness of the thin-sheet material. The equation to calculate rotational stiffness is empirically written as

$$K_l = \frac{L_F}{L^*} \cdot \frac{Et^3}{12(1-\nu^3)} \tag{1}$$

where E and ν are the Young's modulus and Poisson's ratio of material, and t is the thickness of panels. L^* is the length scale parameter which relates the bending of fold lines to the bending of initially flat sheets.

The stiffness K_l is then dependent on L^* and there is no theoretical basis for determining the exact value of L^*. Therefore, a sensitivity analysis is performed (Fig. 3(*b*)) by compressing tubes of 52%, 72%, and 95% extension with different length scales, $L^* = 8$, 50, 500, 1000 mm. As the response curves are relatively close to each other for substantially different length scales, we determine that the global crushing behavior is not sensitive to the local fold stiffness. This phenomenon occurs because the axial crushing is mainly influenced by the constrained geometry from the rigid end plates rather than the local bending stiffness.

Based on the material tests, the elastoplastic constitutive relationship for the polyester material used in the numerical simulation can be modeled as follows:

$$\sigma(\text{MPa}) = \begin{cases} 4400\varepsilon, & \varepsilon < \varepsilon_y = 0.0227 \\ 153.86(\varepsilon - \varepsilon_y) + 100, & \varepsilon_y \le \varepsilon \le 0.15 \\ 120, & 0.15 \le \varepsilon \end{cases} \tag{2}$$

Experimental Methods. Quasi-static uniaxial compression tests of locked zipper tubes are used to explore the nonlinear force–displacement behavior of these systems. First, a set of tensile coupon tests were performed to verify the elastic modulus of the polyester sheets and to test the strength of the adhesive connections. The stress–strain relationships of the coupons are used for the numerical simulations and provide background on the validity and limitations of the experimental tests.

A specialized grip (Fig. 4(*a*)) is fabricated to connect the locked zipper tubes to the test machine, where the tube endplates fit within voids of the grips and are adhered with plastic tape to stay in place. This configuration allows the test machine to apply a compressive force to the locked zipper tubes without restricting rotation at the top. An Instron 5969 dual column axial testing frame is used for the testing with a 1000 N load cell attached to the top grip to record the reaction force. The displacement of the load cell is controlled and recorded by the machine. A testing rate of 25.4 mm/min is used for all experimental tests in this study. Through the numerical simulation, we showed that even at fast loading rates (completing the analysis in 20 ms) the internal dynamics are insignificant when compared to the nonlinear crushing behaviors.

Drop tests are carried out to explore the dynamic properties of locked zipper tubes under a low-energy scenario. The displacement is recorded by tracking a laser pointer attached to the top of the constrained zipper tubes using a high-speed camera. The setup for the dynamic experiments is shown in Figs. 4(*b*) and 4(*c*). The tests are built into a vertical track with T-slot parts (80/20 Inc.). A slider which can move vertically along the track was used to hold the zipper tubes. Horizontal movement at the top of the tubes was restricted by additional sliders while still allowing for vertical movement of the tube (Fig. 4(*b*)). Two tubes can be accommodated on the slider and tested under the same conditions. They are dropped simultaneously and the sliders for horizontal restriction are the same for both tubes. A lighting system is provided to illuminate the devices in order to capture high-quality images with a high-speed camera (Photron INC., FASTCAM SA5). Videos are recorded at a frame rate of 2000 frames per second. For the quantitative results, displacement is tracked using the high-speed images. Tracking of the objects was most precise when measured from two laser pointers attached to the top of the zipper tubes (Fig. 4(*c*)). These laser pointers provided precise point-based locations for the tube tops through the duration of the drop test.

Results

Quasi-Static Axial Tests. Zipper tubes locked at three different states of extension, 52%, 72%, and 95%, are tested with a

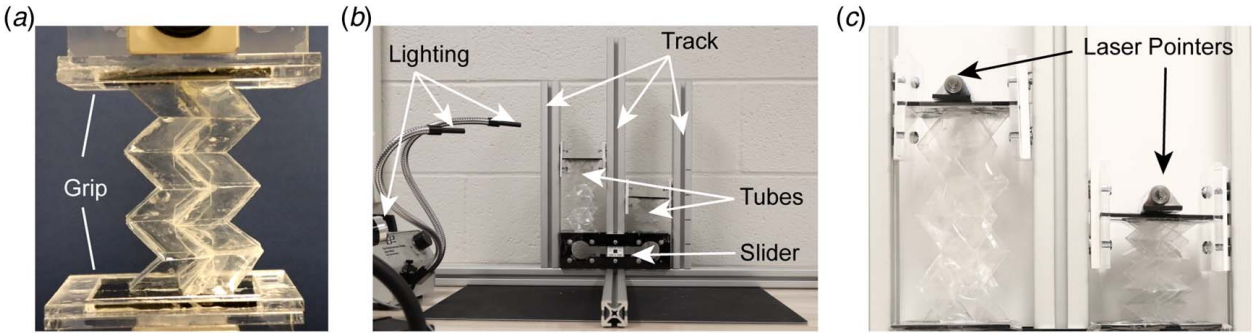

Fig. 4 Experimental methods. (*a*) A locked zipper tube in a quasi-static test. (*b*) The drop test frame. (*c*) Two laser pointers at the top of the tubes allow for accurate tracking of the position with a high-speed camera.

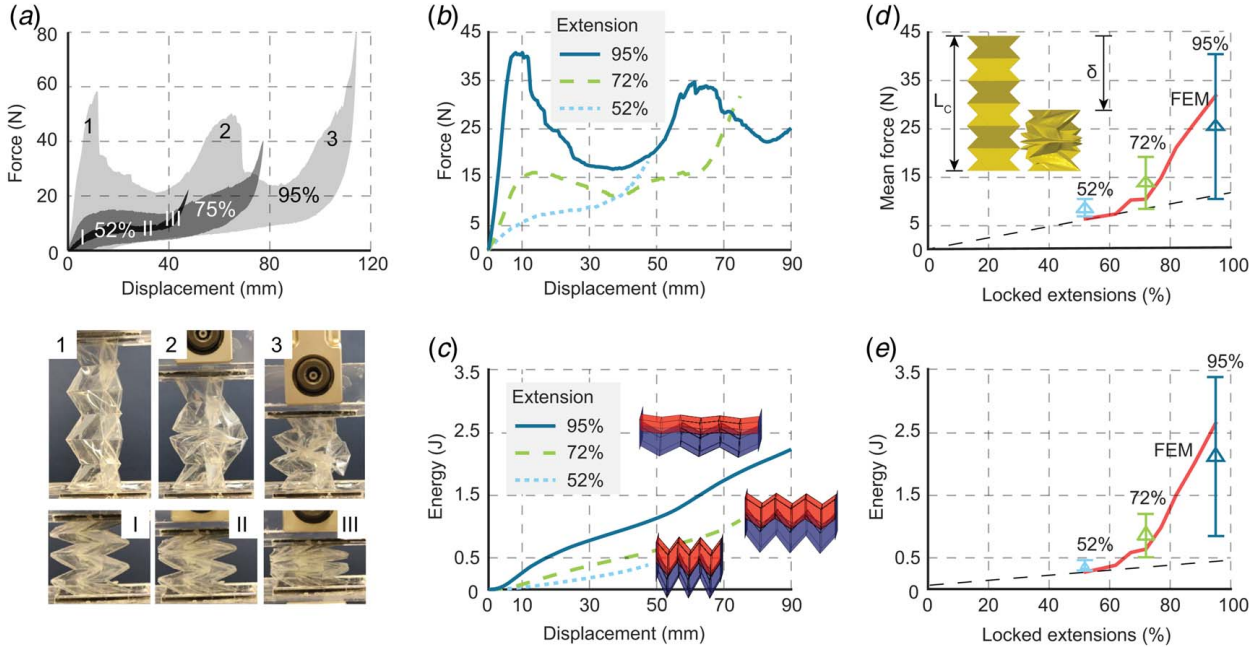

Fig. 5 Quasi-static axial loading response of locked tubes. (*a*) Load–unload cycle response of tubes extended to 52%, 72%, and 95% (top) and corresponding experimental photos for the 95% and 52% extensions (bottom). The shaded area is the dissipated energy during a load–unload cycle. (*b*) Mean value of loading responses from seven experiments for each extension. (c) Mean value of energy absorption from seven experiments for each extension. (*d*) Comparison of mean force between experimental testing and numerical FEM simulation (for a crushing distance $\delta/l_c = 50\%$). (*e*) Comparison of absorbed energy between experimental testing and numerical FEM simulation (for a crushing distance $\delta/l_c = 50\%$).

load–unload cycle (Fig. 5(*a*), Movie S1 available in the Supplemental Materials on the ASME Digital Collection), where the shaded area denotes the dissipated energy during a load–unload cycle. The initial stiffness increases with the extension of the tubes (i.e., 1 N/mm for the 52%, 1.8 N/mm for the 72%, and 6.5 N/mm for the 95%). The tubes at 52% extension show a nearly elastic response and recovery; and thus, little energy is dissipated. During loading, there is some elastic buckling and minor yielding (point no. I), followed by a plateau (point No. II), and finally some densification of the tube (point no. III). Upon recovery, the force–displacement response is nearly identical with the buckled locations recovering to the initial configuration. For the tubes with 52% extension, most of the deformations occur as recoverable buckling and local bending around fold lines which follows the one DOF kinematics of the origami. The tubes locked at higher extensions have a more nonlinear force–displacement response because more panel deflection, buckling, and local yielding occur. The force–displacement results for the zipper tubes at 95% extension show three peaks during the loading process. Before the first peak, the zipper tubes have a linear elastic response to the axial loading. Due to the buckling and local cracking in the adhesive around fold lines, the force drops sharply at point no. 1. As the loading is continued, localized contact occurs at the central segments, which leads to another peak in the force–displacement curve (point no. 2). More buckling around end-segments of the tube brings the force down until the whole structure becomes densified (point no. 3). As the system is unloaded, it has a low stiffness and recovers near linearly (from 80 to 0 mm displacement). The response of the tube with 72% extension is between the two other cases. Buckling, yielding, and local bending around fold lines are affecting the global responses simultaneously in the tube with 72% extension. Buckling and yielding induce a drastic change in the forces and non-recoverable deformations, whereas the local bending will

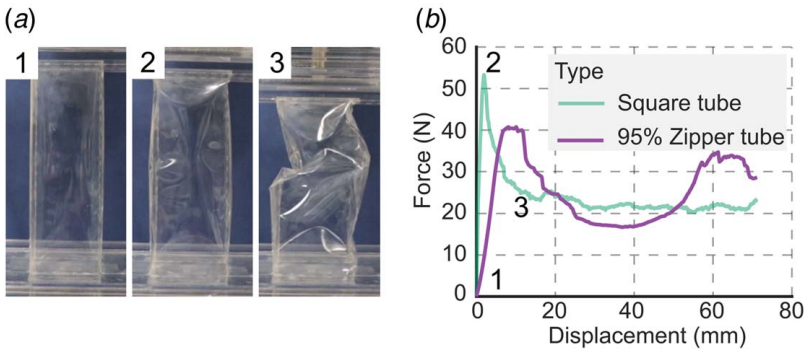

Fig. 6 Comparison of the energy absorption behavior between prismatic tubes and locked zipper tubes of the same length. (*a*) Experimental photos of prismatic square tubes, the numbering corresponds to part (*b*). (*b*) Mean value of loading responses from seven experiments for prismatic tubes and locked zipper tubes at 95% extension.

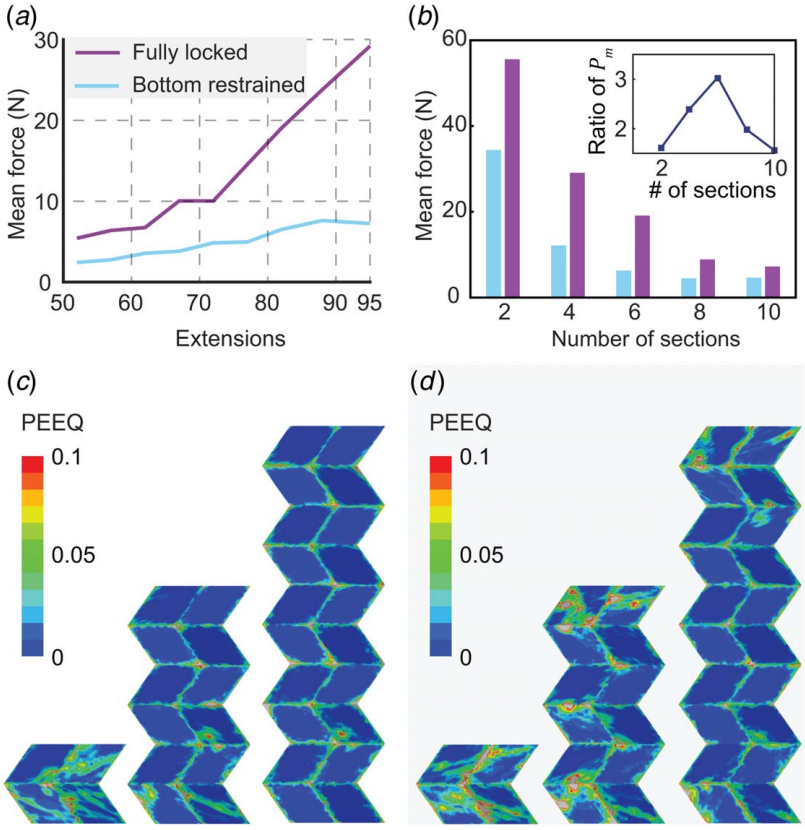

Fig. 7 Comparison of the energy absorption behavior between zipper tubes that are locked on both ends and zipper tubes that are restrained only on the bottom end. Comparison of mean force for (*a*) different extensions and (*b*) different number of segments, while the extension is set to be 82%. The crushing distance $\delta/L_c = 50\%$. Plastic deformation for (c) the bottom-restrained and (*d*) the fully locked tubes with different number of segments deployed to 82% extension (the equivalent plastic strain, PEEQ, is plotted on the undeformed shape).

increase the forces and recover after unloading. A combination of these opposing effects distinguishes the loading response from the nearly elastic behavior of the tube with 52% extension or the fluctuating forces of the tube with 95% extension.

To verify the overall behavior with respect to extension, seven individual tests are performed for each of the three cases. The overall force–displacement for the three sets of tests is similar to those shown in Fig. 5(*a*). The systems with low extension (52%) have a nearly recoverable response, those at a high extension (95%) have three peaks, and the third set (72%) again fall in the middle. The load–displacement response for each set of tubes is averaged and presented in Fig. 5(*b*). The overall behavior is again influenced by the extensions. The tubes with larger extension exhibit a larger axial stiffness, a higher peak force for crushing, and are able to provide a longer crushing distance before densification.

As illustrated in Fig. 1(*a*), the absorbed energy for each test is characterized as the area underneath the force–displacement curve. Figure 5(*c*) shows the absorbed energy versus the crushing distance for the three sets of experimental tests (each set is averaged). This plot shows another tunable behavior benefited from the deployable property of these systems. The tubes with larger extensions have higher levels of energy-absorbing capability even for the same crushing distance (slopes of lines in Fig. 5(*c*)). From the quantitative comparison of mean values of energy absorption, the locked zipper tubes extended to 95% can absorb 2.3 J while those at 52% absorb less than 0.4 J. However, the mean forces and peak forces also increase with the extension. In summary, the behavior obtained from quasi-static tests show that the axial response including stiffness, peak force for crushing, and total energy absorption can be changed dramatically for the same tube design. By deploying and locking the tubes at different extensions, it is possible to tune the behavior without changing the system design.

Finite element numerical simulations are performed for the same range of tube extensions, and the results are compared with experimental results in terms of the mean reaction force and absorbed energy (Figs. 5(*d*) and 5(*e*)). The large variation of experimental results comes from the limited specimens. For each deployment ratio, we made seven samples for the quasi-static compressions. The variation can be narrowed by testing more samples.

These results are obtained when we compare the systems over a crushing distance of $\delta/L_c = 60\%$ of the total length of locked zipper tubes (see schematic in Fig. 5(*d*)). Comparing over only a portion of the crushing distance (50–80%) provides a more reasonable comparison, because the finite element models substantially overestimate forces and energy absorption in the densification regime. For the limited range, the mean forces and total energies are in reasonable agreement with those obtained from the compression experiments. Additionally, the overall trends are similar and show that the extension can be used to increase the forces and the total amount of energy absorbed. Finally, the increase of energy absorption from extending the tubes is substantially faster than a linear growth (dashed line in Fig. 5(*e*)). In other words, if the tube is already deployed past 50% extension, a small additional extension will result in much higher forces and energy absorption.

Benchmark Comparison. Seven conventional square tubes of the same length and cross-sectional area are tested to set a

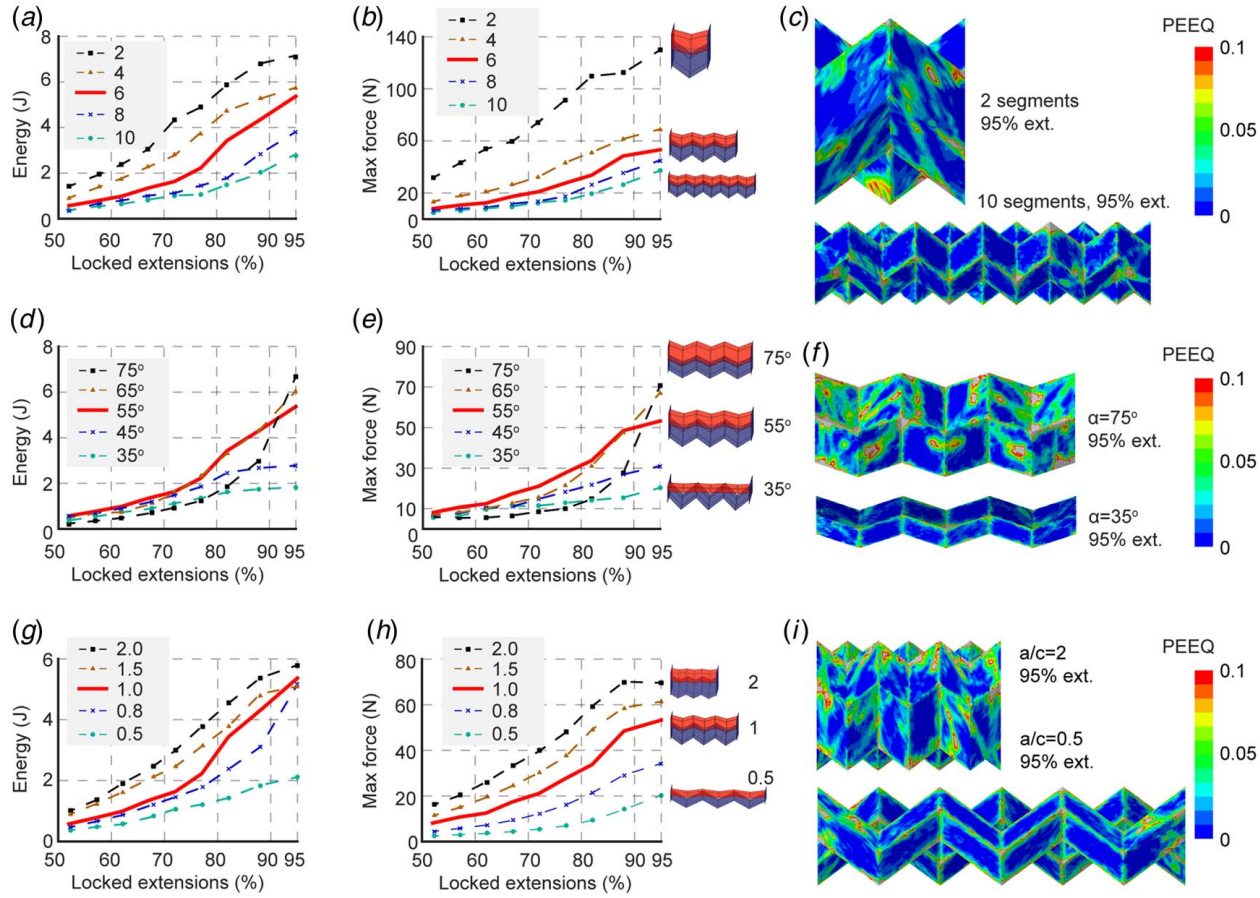

Fig. 8 Parametric variation of tube geometry. (*a*) Energy absorption and (*b*) maximum force for tubes with different number of segments. (c) Plastic deformation for two tubes with a different number of segments (PEEQ is plotted on the undeformed shape). Distributed panel plastification is observed for tubes with only two segments, whereas most plastic deformation occurs around fold lines for tubes with ten segments. (*d*) Energy absorption and (*e*) maximum force for tubes with different vertex angles. (*f*) Plastic deformation for tubes with different vertex angles deployed to 95% extension (PEEQ is plotted on the undeformed shape). Distributed panel plastification is observed for tubes with a vertex angle of $\alpha = 75$ deg, whereas most plastic deformation happens around fold lines for tubes with a vertex angle of $\alpha = 35$ deg. (*g*) Energy absorption and (*h*) maximum force for tubes with different aspect ratios. (*i*) Plastic deformation for tubes with different aspect ratios deployed to 95% extension (PEEQ is plotted on the undeformed shape). Distributed panel plastification is observed for tubes with an aspect ratio of $a/c = 2$, whereas most plastic deformation happens around fold lines for tubes with an aspect ratio of $a/c = 0.5$.

benchmark for evaluating the relative energy-absorbing behavior of the locked zipper tubes. The square tube is selected as a representative of the conventional thin-walled prismatic energy absorbers, because those devices have similar loading responses where the critical buckling causes a high initial peak force and subsequent sharp decrease. These square tubes are fabricated with the same polyester sheets as the locked zipper tubes, where the total amount of material used and the axial length of the squared-tube are equal to the locked zipper tubes at 95% extension. Both ends of the prismatic tube are glued to two square acrylic plates to restrain the translational movement (Fig. 6(*a*)). These prismatic tubes are tested using the same loading procedure as the locked zipper tubes and the mean loading responses are plotted in Fig. 6(*b*) for the prismatic tubes and the locked zipper tubes at 95% extension. The energy-absorbing characteristics are compared over the whole crushing distance of $0.5L_c = 72.5$ mm, where L_c is the initial length of both tubes. The comparison shows that initial peak force of the locked zipper tubes (40.7 N) is 23.6% lower than the initial peak force of the prismatic tubes (53.3 N), whereas mean crushing force of the locked zipper tubes (24.9 N) is slightly higher than the mean crushing force of the prismatic tubes (23.9 N). These results show that the zipper-coupled origami pattern offers similar advantages for energy absorption as those presented with other origami inspired designs [2] and can provide an overall comparable response to prismatic tubular systems. Notice that if the comparison is carried out over a shorter crushing distance (e.g., $0.14L_c \approx 20$ mm), the mean crushing force of the square tube (29.5 N) will be greater than that of the zipper tube (28.8 N). However, to absorb more impact energy, an thin-walled tube is typically crushed over a longer portion of the initial length (e.g., half of the initial length or more).

Table 1 The ratio of the amount of energy absorbed at 95% extension to the corresponding peak force ($\delta \cdot P_m/P_{max}$)

Number of segments	2	4	6	8	10
$\delta \cdot P_m/P_{max}$ (10^{-1} J/N)	0.55	0.83	1	0.84	0.76
Aspect ratio, a/c	0.5	0.8	1.0	1.5	2.0
$\delta \cdot P_m/P_{max}$ (10^{-1} J/N)	1	1.5	1	0.83	0.83

Influence of the End Constraints. Figure 2(*d*) shows that a zipper tube that is locked on both ends can offer significantly more stiffness than an unrestrained tube, and is thus suitable for energy absorption. The numerical study of energy characteristics is now extended to zipper tubes that are only restrained on the bottom, and the locking at the top plate is released. The FE

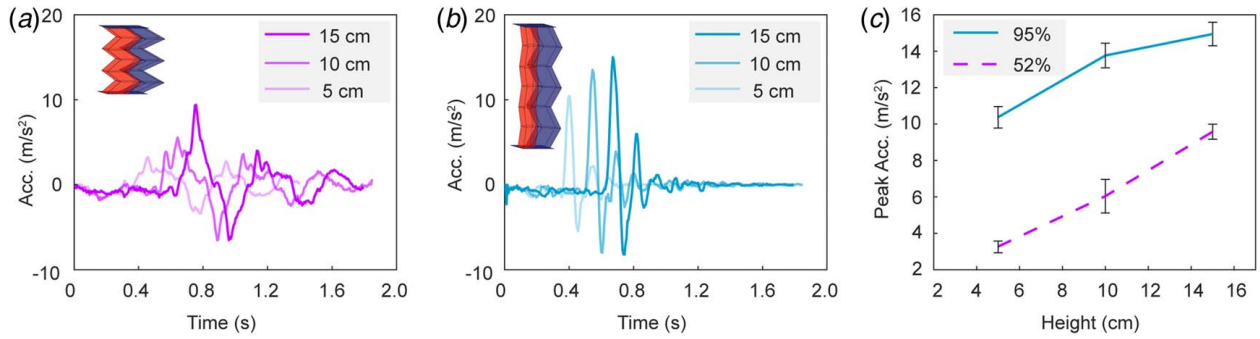

Fig. 9 Drop tests demonstrating peak accelerations in a low-energy impact scenario. (*a*) Time history of acceleration for tubes with an extension of 52% and (*b*) tubes with an extension of 95%. (*c*) The peak accelerations after collision versus drop heights. The 90% confidence intervals are indicated with vertical bars and are derived from four repeated tests.

model of the bottom-restrained zipper tube is built with same geometry as the fully locked tube, while the top plate now only serves as a moving plate to compress the tube. Finite element simulations are performed for the same range of extensions from 52% to 95%, and the mean crushing forces are compared with those of fully locked tubes (Fig. 7(*a*)). The results compare the tubes over a crushing distance of $\delta/L_c = 50\%$ of the total length. Both trends show that the mean forces (P_m) increase with the axial extension, while the fully locked tubes have a higher P_m over the whole range of extensions. The fully locked zipper tube can absorb more energy because the restraint from the top plate results in more panel crushing within the segments that are close to the top.

For zipper tubes with different number of segments, the top restraint has a different level of influence on the overall energy behavior. Keeping the panel geometry to be the same, zipper tubes with different number of segments are compressed from 82% extension, and their mean forces are shown in Fig. 7(*b*). With more segments in the tube, the mean force decreases for both the fully locked and the bottom-restrained tubes, because with more segments there is more kinematic deformation and less crushing. However, the difference between the mean forces, quantified as the ratio of the fully locked P_m to the bottom-restrained P_m, varies with the number of segments (inset in Fig. 7(*b*)). The ratio first increases then decreases with the number of section, and it reached the peak for six segments. The trend of this ratio is related to the distribution of crushing in the two different locked cases, which can be explored through the equivalent plastic strain, PEEQ, in the systems (Figs. 7(*c*) and 7(*d*)). With only two segments, the case with only the bottom restraint still provides substantial constraint to the kinematics of the tube, inducing similar panel crushing and plastic strain to those of the fully locked tube. Thus, the fully locked P_m is only 1.6 times as high as the bottom-restrained P_m. For the bottom-restrained tube with six segments, the top panels are much less restrained and do not experience crushing, while the fully locked tube can provide restraints and cause more panel crushing. Thus the ratio of P_m increases to 3. Furthermore, with ten segments in the tube, the majority of the panels in both tubes will follow the kinematic folding motions of the creases, regardless of the existence of the top restraint. The ratio of P_m drops back to 1.6, which implies that the energy absorption is not significantly improved by adding the top restraint.

Parametric Study. The finite element simulations are extended to conduct a parametric study where the geometry of locked zipper tubes is varied. From the parameters used in the geometric design of zipper tubes, the number of segments N, the vertex angle α, and the aspect ratio a/c (Figs. 2(*a*) and 2(*b*)) result in differences in the system performance. To enable a fair comparison within the parametric study, the total material cost and the shell thickness of the zipper tubes are kept the same for all cases. As the number of segments is changed, the size of panels (variables a and c) changes such that the material cost remains the same. The crushing percentage (δ/L_c) is set to be 80% for all simulations. Changing the number of segments does not change the overall kinematics of the tubes. The vertex angle and the aspect ratio characterize the planar geometry of the Miura-ori pattern, which affects the global shape of the system. Changing the vertex angle or the aspect ratio does not affect the size of the panels (variables a and c). The vertex angle does affect the folding kinematics of the system where tubes with higher α change their shapes to essentially square-like tubes when fully deployed. The aspect ratio also alters the folding kinematics, where a larger aspect ratio defines a shorter and more dense zipper tube. The crushing characteristics of the different parametric cases are compared in terms of the energy absorption and the maximum force $P_{\max}$ (Fig. 8).

The Number of Segments. When increasing the number of segments in a tube, both the absorbed energy and the maximum force decrease (Figs. 8(*a*) and 8(*b*)). The general trends are similar to those observed in the experiments, and the force/energy characteristics with respect to deployment remain aligned for the different number of segments (lines do not overlap). To compare the efficacy of these systems as energy absorbers, we compare the ratio of the amount of energy absorbed at 95% extension to the corresponding peak force ($\delta \cdot P_m/P_{\max}$, summarized in Table 1). All these systems use the same amount of material, so if more energy absorption is desired, then the design with the fewest segments should be used (Fig. 8(*a*)). However, if it is also desirable to mitigate the peak crushing forces, then tubes with six segments provide the maximum energy absorbed for the lowest relative peak force (Table 1). These trends are a result of the strain distribution and crushing behavior of the origami tubes (see Fig. 8(*c*), where the PEEQ represents the equivalent plastic strain status). For the most part, we see the high strains to be happening around diagonals. Additionally, we see the high strains happening at the vertices. The only case where we see islands of high strains is when there are only two segments in the zipper tube. All the tube panels are subjected to constraints from the rigid plates. The local rotations are restrained, leading to crushing and higher strains. For the zipper tube with more segments, portions in the middle of the tube have less restriction and can experience a more controlled buckling that also involves kinematic deformation of the system. These buckling characteristics and the plasticity distributions could allow for more advanced designs of the structures, where the number of segments could be used to design the mean to maximum force ratio in the system.

The Planar Geometry. Both the vertex angle α and the aspect ratio a/c can change the planar geometry of the Miura-ori pattern.

When varying the vertex angles, the energy absorption properties with respect to the system extension show different nonlinear trends (Figs. 8(*d*) and 8(*e*)). For a tube with a vertex angle of $\alpha = 75$ deg, the energy absorption increases from 0.24 J at 50% extension to 6.76 J for a 95% extension (28 times increase). On the other

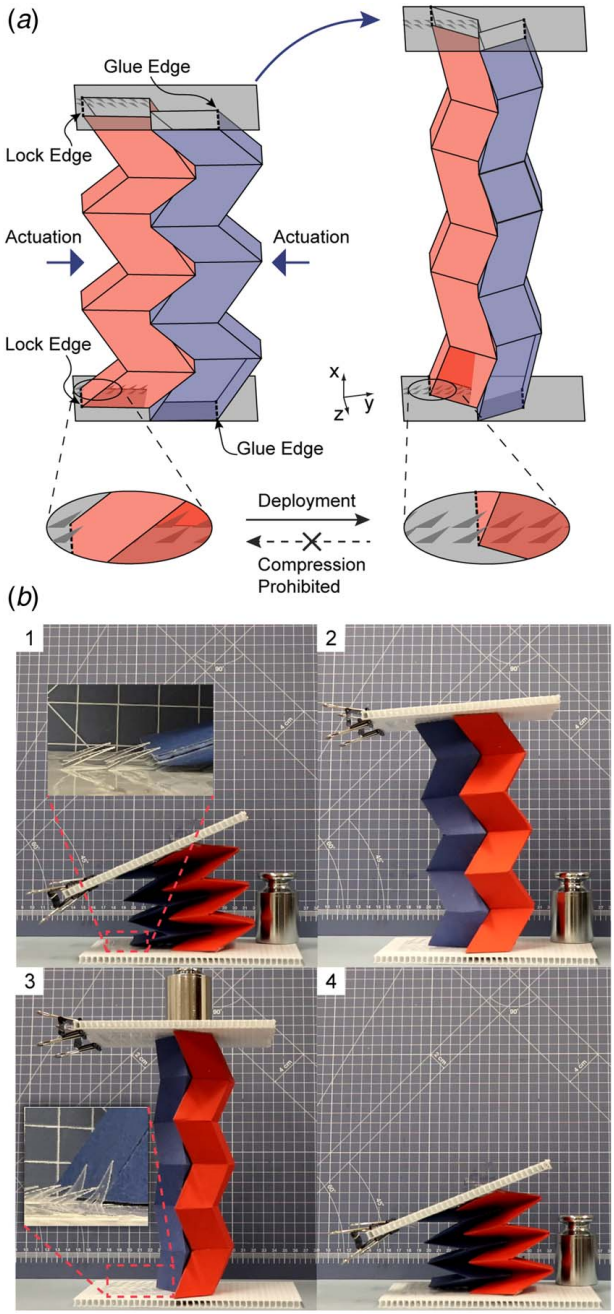

Fig. 10 Self-locking of the zipper-coupled tube. (*a*) A tube at 72% extension is deployed to 95% extension by squeezing the sides. Panels on the ends are locked into one-way inclined ridges that are bonded onto the rigid plates. The lock edge is parallel to the glued edge. (*b*) Corresponding experimental photos of the deployment and locking. The tube is (1) at the initial state; (2) deployed and locked at around 70% extension; (3) deployed and locked at around 90% extension, and a mass of 500 g is supported on the top; (4) retracted to the initial state by releasing the locking ridges from the tube edge. The insets show the locking ridges at the initial state (1) and a deployed state (3). See Movie S4 available in the Supplemental Materials on the ASME Digital Collection.

hand, the trend for a smaller vertex angle is smoother without such a drastic variability. For example, the tube with $\alpha = 35$ deg has an energy absorption of 0.37 J at 50% extension and only increases to about 1.82 J at 95% extension (only a 4.9 times increase). The maximum forces follow these same general trends where higher vertex angles result in higher variability with extension. These results show that the vertex angle can be used to control *how tunable the system is*. The change in the energy absorption trends relate to the kinematics of the systems. When the tubes are deployed to a smaller extension (e.g., 50%), the crushing of all tubes follows the fold kinematics and little energy is absorbed. When deployed to higher extensions (above 90%), crushing the tubes with large vertex angles engages local panel deformations and distributes plasticity throughout the system, while crushing tubes with small vertex angles still follow the fold kinematics (Fig. 8(*f*)).

When increasing the aspect ratio *a*/*c* of the tube panels, both the absorbed energy and the maximum force increase (Figs. 8(*g*) and 8(*h*)). The ratio of the energy absorption at 95% extension to the corresponding peak force ($\delta \cdot P_m/P_{\max}$) is compared to show the efficacy (Table 1), and the tubes with aspect ratio around 1.0 offer the highest efficacy. The change of the energy absorption and the max force is related to the global shape difference (Fig. 8(*i*)). The tubes with large aspect ratio are shorter and more dense (Fig. 8(*i*)), i.e., have more amount of material in a unit longitudinal length. When the tubes are compressed, the same crushing distance results in more material deformation in the tubes with large aspect ratio. Furthermore, for the zipper tubes with large aspect ratio, the tube panels also have more restriction from the rigid plate due to the smaller longitudinal length, causing higher strains within the tube panels (Fig. 8(*i*)). Thus, the energy absorption and the max force both increase with the aspect ratio based on the above two effects.

Drop Tests and Dynamic Analyses. Mechanical properties such as axial stiffness and yielding forces can be extracted from the quasi-static loading response, whereas the ability of the absorber to provide buffering during impact can be characterized by exploring the acceleration time history after a free drop and collision. A small mass is attached to the top of a locked tube to provide enough impact, and the drop frame (Fig. 4(*b*)) is used to test the buffering capabilities. The tests are performed at three different heights and the peak acceleration versus drop height are calculated (Figs. 9(*a*)–9(*c*)). The acceleration time history is calculated by twice differentiating the displacement data. The longer constrained zipper tubes (95% extension) result in a larger peak acceleration after the collision when compared to tubes with the same geometry but shorter extension. For the drop test from a height of $h = 5$ cm, the peak acceleration for a zipper tube at 52% extension averages at 3.5 m/s^2, whereas the peak acceleration for tubes at 95% can reach 10 m/s^2. Similar relations can also be observed with different drop heights. The peak acceleration during a collision is correlated to the damage that can be transmitted to protected objects. A lower peak acceleration (52% extension) corresponds to better protection, and a higher peak acceleration (95% extension) means more serious damage. Although the friction in the system is not negligible, it does not affect the comparison between the tubes, as they are dropped simultaneously with the same setup (discussed in the experimental methods).

Dynamic buffering capability is also demonstrated qualitatively using drop tests with (i) two measuring cylinders containing 2 cm of colored water which are placed on locked zipper tubes with extensions of 52% and 95% (Movie S2 available in the Supplemental Materials on the ASME Digital Collection) and (ii) eggs on top of a 52% locked zipper tube and the slider (Movie S3 available in the Supplemental Materials on the ASME Digital Collection).

In this low-energy scenario, these structures with extension of 95% do not crush during the test, and their high stiffness causes the higher accelerations. On the other hand, the tubes with a 52% extension have a substantially lower stiffness and remain nearly elastic (even when slight crushing and nonlinearity occurs (Fig. 5(*a*)).

Locking Mechanism

In this subsection, we show a locking mechanism inspired by zip ties that allows the deployment and subsequent self-locking of the

zipper-coupled tubes (Fig. 10). On each end of the zipper-coupled tube, there is one edge that is glued to the end plate, and a parallel edge that is able to move and engage with the locking mechanism (Fig. 10(*a*)). As the zipper tube deploys in the x direction, the tube dimension in the y direction shrinks, and the two parallel edges move closer together. The deployment and self-locking can then be realized by allowing the two edges to approach each other, but creating locking components that prevent them from moving apart again. The zip-tie inspired mechanism can fulfill this function. Two racks of inclined ridges are bonded onto each rigid plate, and the ridges are set to be inclined toward the direction along which the parallel pair will get closer (Fig. 10(*a*)). The glued edge is bonded to the rigid plate to restrain relative translations, and the lock edge serves as a ratchet. As the tube extends, the lock edge travels past each ridge without much resistance. If the lock edge moves back in the opposite direction, it will go under the ridges, and its motion will be prohibited by the inclined ridge. Thus if the tube is compressed, the locking mechanism will prevent it from folding back to a flat state.

A physical self-locking example is shown in Fig. 10(*b*) and Movie S4 available in the Supplemental Materials on the ASME Digital Collection. With two built-in racks of inclined ridges on the plastic plates, the zipper-coupled tube can deploy and stay at ~70% extension (Fig. 10(*b*), part 2) and ~90% extension (Fig. 10(*b*), part 3). A mass of 500 g can be supported by the self-locking tube (Fig. 10(*b*), part 3), demonstrating the strength of the zip-tie locking mechanism. Finally, by rotating the plastic plates about the glued edge, the racks of inclined ridges will detach from the tube, and the tube can come back to its initial state (Fig. 10(*b*), part 4).

Concluding Remarks

This paper introduces a concept for using origami tubes as deployable and adaptable energy-absorbing devices. Experimental and numerical studies of the deployable tubes demonstrate the tunable characteristics. Locking the tubes changes the system from being elastically deployable to becoming stiff structures that require crushing to compress longitudinally (nine times stiffer for a tube at 72% extension). Axial quasi-static experiments of the tubular structures made from polyester sheets demonstrate that the stiffness, system forces, and energy absorption all increase as the system is deployed. The quantitative increase of these properties is nonlinear with respect to extension of the system. Numerical simulations of the crushing are in reasonable agreement with the experimental results. Both studies show similar values for the force–displacement characteristics and the overall system trends with respect to the extension. The improvement of using the locked zipper tubes as energy absorbers is verified by comparing the crashworthy behavior with that of prismatic tubes. A numerical parametric study indicates that tubes with fewer segments (fewer panels and folds) will result in more plasticity throughout the structure resulting in higher energy absorption and peak forces. These results demonstrate the importance of effectively locking the thin-sheet structure to absorb energy through crushing. Structures with six segments have an optimal balance when comparing the total energy absorption to the peak force. For these systems, it is important to lock both ends of the tube, while locking only one will provide only about a third of the energy absorption. A parametric study on the design of the planar tube geometry showed that the vertex angle can control the nonlinearity of the relationship between energy absorption and extension, or in other words how tunable the system is. Another parametric study on the planar geometry suggests that the energy absorption increases with the panel aspect ratio, where a short and dense tube will crush with more plasticity. Given a low-energy impact, a set of experimental dynamic drop test show that the tubes can offer different levels of buffering when locked at different extensions. Finally, a physical model based on the zip-tie mechanism is introduced to demonstrate self-locking of the tube after deployment.

In comparison with the conventional thin-walled tube of identical material cost, the proposed zipper tube shares similar loading responses as those of other origami energy absorbers [2,6]: lower peak force and more energy absorption. Moreover, the zipper tube also owns the potential to tune the energy-absorbing behavior by deploying to different extensions. For vehicle applications, we expect that the deployable energy absorbers can work with speed sensors that detect the incoming collision. Generally, the absorbers should be deployed to a longer extension for a higher speed to absorb as much impact energy as possible. For a relatively lower speed, the absorbers should be deployed to a shorter extension to reduce the peak force. A set of sensors, decision making methods, and control algorithms will be required to effectively implement and use the active energy absorption.

The work presented here is a proof-of-concept for the deployable and adaptable energy-absorbing systems and is thus limited in nature. First, innovation and improvement are needed in the materials, design, and scalable fabrication of the deployable origami tubes [20]. Next, it is important to resolve methods for rapid deployment mechanism to allow real-time responsive behavior. An inflatable bladder within the origami tubes [21] driven by a chemical reaction similar to an airbag could be suitable for rapid deployment and tuning. Using fabric-polyester for fabrication can increase the life-span robustness [22]. Calculation of the energy absorption per unit volume versus density would enable the comparison to other materials, using the standard Ashby map [23]. We are hoping that we can create a mechanism in the future, enabling the tunable locking and deployment of the system.

Acknowledgment

We are thankful to Drs. Lynch, Kerkez, El-Tawil, and Li for helpful discussion and sharing of laboratory equipment used in this work.

Funding Data

- The authors acknowledge support from the ZF Automotive Research Award and the Office of Naval Research (Grant No. N00014-18-1-2015).

Conflict of Interest

There are no conflicts of interest.

Data Availability Statement

The datasets generated and supporting the findings of this article are obtainable from the corresponding author upon reasonable request.

References

[1] Wierzbicki, T., and Abramowicz, W., 1983, "On the Crushing Mechanics of Thin-Walled Structures," ASME J. Appl. Mech., **50**(4a), pp. 727–734.

[2] Ma, J., and You, Z., 2013, "Energy Absorption of Thin-Walled Square Tubes With a Prefolded Origami Pattern—Part I: Geometry and Numerical Simulation," ASME J. Appl. Mech., **81**(1), p. 011003.

[3] Yang, K., Xu, S., Zhou, S., and Xie, Y. M., 2018, "Multi-objective Optimization of Multi-cell Tubes With Origami Patterns for Energy Absorption," Thin-Walled Struct., **123**, pp. 100–113.

[4] Ma, J., Hou, D., Chen, Y., and You, Z., 2016, "Quasi-Static Axial Crushing of Thin-Walled Tubes With a Kite-Shape Rigid Origami Pattern: Numerical Simulation," Thin-Walled Struct., **100**, pp. 38–47.

[5] Xiang, X. M., Lu, G., and You, Z., 2020, "Energy Absorption of Origami Inspired Structures and Materials," Thin-Walled Struct., **157**, p. 107130.

[6] Yang, K., Xu, S., Shen, J., Zhou, S., and Xie, Y. M., 2016, "Energy Absorption of Thin-Walled Tubes With Pre-folded Origami Patterns: Numerical Simulation and Experimental Verification," Thin-Walled Struct., **103**, pp. 33–44.
[7] Qi, J., Li, C., Tie, Y., Zheng, Y., and Duan, Y., 2021, "Energy Absorption Characteristics of Origami-Inspired Honeycomb Sandwich Structures Under Low-Velocity Impact Loading," Mater. Des., **207**, p. 109837.
[8] Filipov, E. T., Tachi, T., and Paulino, G. H., 2015, "Origami Tubes Assembled Into Stiff, Yet Reconfigurable Structures and Metamaterials," Proc. Natl. Acad. Sci. U.S.A., **112**(40), pp. 12321–12326.
[9] Meloni, M., Cai, J., Zhang, Q., Sang-Hoon Lee, D., Li, M., Ma, R., Parashkevov, T. E., and Feng, J., 2021, "Engineering Origami: A Comprehensive Review of Recent Applications, Design Methods, and Tools," Adv. Sci., **8**(13), p. 2000636.
[10] Surjadi, J. U., Gao, L., Du, H., Li, X., Xiong, X., Fang, N. X., and Lu, Y., 2019, "Mechanical Metamaterials and Their Engineering Applications," Adv. Eng. Mater., **21**(3), p. 1800864.
[11] Shan, S., Kang, S. H., Raney, J. R., Wang, P., Fang, L., Candido, F., Lewis, J. A., and Bertoldi, K., 2015, "Multistable Architected Materials for Trapping Elastic Strain Energy," Adv. Mater., **27**(29), pp. 4296–4301.
[12] Wo, Z., Raneses, J. M., and Filipov, E. T., 2021, "A Numerical and Experimental Study on the Energy Absorption Characteristics of Deployable Origami Tubes," Vol. 10: 45th Mechanisms and Robotics Conference (MR) of International Design Engineering Technical Conferences and Computers and Information in Engineering Conference, Virtual, Online, Aug. 17–19, p. V08BT08A029.
[13] Miura, K., 1985, "Method of Packaging and Deployment of Large Membranes in Space," Inst. Space Astronaut. Sci., **618**, pp. 1–9.
[14] Schenk, M., and Guest, S. D., 2013, "Geometry of Miura-Folded Metamaterials," Proc. Natl. Acad. Sci. U.S.A., **110**(9), pp. 3276–3281.
[15] Zhang, Q., Wang, X., Cai, J., Ren, Z., and Feng, J., 2021, "Development of Kinetic Origami Canopy Using Arc Miura Folding Patterns," J. Build. Eng., **43**, p. 103116.
[16] Filipov, E. T., Tachi, T., and Paulino, G. H., 2019, "Coupled Origami Tubes for Stiff Deployable Cantilevers," Vol. 5B: 43rd Mechanisms and Robotics Conference of International Design Engineering Technical Conferences and Computers and Information in Engineering Conference, Anaheim, CA, Aug. 18–21, p. V05BT07A023.
[17] ABAQUS, 2010, "Abaqus FEA, Version 6.10 Documentation."
[18] Filipov, E. T., Liu, K., Tachi, T., Schenk, M., and Paulino, G. H., 2017, "Bar and Hinge Models for Scalable Analysis of Origami," Int. J. Solids Struct., **124**, pp. 26–45.
[19] Lechenault, F., Thiria, B., and Adda-Bedia, M., 2014, "Mechanical Response of a Creased Sheet," Phys. Rev. Lett., **112**(24), p. 244301.
[20] Zhao, Z., Wu, J., Mu, X., Chen, H., Qi, H. J., and Fang, D., 2017, "Origami by Frontal Photopolymerization," Sci. Adv., **3**(4), p. e1602326.
[21] Li, S., and Wang, K. W., 2015, "Fluidic Origami With Embedded Pressure Dependent Multi-stability: A Plant Inspired Innovation," J. R. Soc. Interface, **12**(111), p. 0639.
[22] Sharifzadeh, M., Jiang, Y., Khodambashi, R., and Aukes, D., 2020, "Increasing the Life Span of Foldable Manipulators With Fabric," Vol. 10: 44th Mechanisms and Robotics Conference (MR) of International Design Engineering Technical Conferences and Computers and Information in Engineering Conference, Virtual, Online, Aug. 17–19, p. V010T10A087.
[23] Yuan, S., Chua, C. K., and Zhou, K., 2019, "3D-Printed Mechanical Metamaterials With High Energy Absorption," Adv. Mater. Technol., **4**(3), p. 1800419.